

Analysis of Hydrodynamic Forces Acting on a Rolling Body by Using Navier-Stokes Solver

Navier-Stokes ソルバーを用いた浮体のロール動揺時の流体力の解析

Emma Patricia BANGUN* and Tomoaki UTSUNOMIYA**

エマ パトリシア バングン・宇都宮智昭

* Student Member, M. of Eng., Dept. of Civil & Earth Resources Eng., Kyoto University

** Member, Dr. of Eng., Associate Professor, Dept. of Civil & Earth Resources Eng., Kyoto University

(Katsura Campus, Nishigyo-ku, Kyoto 615-8540)

This paper presents a numerical method based on the Navier-Stokes equations to evaluate viscous forces acting on a moving body. A cell center based finite volume method for unstructured grids is applied to discretize the computational domain and solve the governing equations. A floating body with or without bilge keels undergoing roll motions at different roll angles is taken as model case. Evaluation of hydrodynamic coefficients due to viscous forces is conducted. The numerical results show that the roll-damping coefficients obtained by using the Navier-Stokes solver are larger than the radiation damping coefficients evaluated by the linear potential theory due to viscous and vortex effect.

Key Words: Navier-Stokes solver, viscous flow, floating structure, rolling motions

1. Introduction

Predicting floating structure motions due to wave and the corresponding hydrodynamic loads is of great importance to the floating structure design and the mooring system. Numerical results from previous studies still fail to predict motions of floating body especially in case of rolling motions. This is due to high non-linearity of rolling motions. Viscous and vortex effects in the fluid are of causes the non-linearity state. Thus, neglecting the fact that the fluid is viscous and the fluid motion is rotational will bring to false prediction on the hydrodynamic loads and lead to inaccurate added mass and damping coefficients.

Potential theory is applicable for motion analysis of the floating body. However the inherent assumptions of potential theory, which are inviscid flow and irrotational fluid motion, are the main reasons of why this method is unfavorable in case of rolling motions. The flow at the corner of hull section is separated and affects the hydrodynamic forces acting on the body. Significant effects occur especially if the body is rectangular-shaped or has sharp corners such as bilge keels fitted on hull sections.

Experimental approach to the evaluation of roll damping due to viscous and vortex-making was presented by Chakrabarti et al.¹⁾. Empirical formulae and/or by the experiment give good approach but the direct numerical evaluation is still more

favorable. Yeung et al.²⁾ and Yeung³⁾ have developed numerical approach called the Free-Surface Random-Vortex Method (FSRVM) for evaluation of the effect of vorticity. Kinnaas et al.⁴⁾ have evaluated the flow around the FPSO (Floating Production, Storage and Offloading vessel) hull section by unsteady Navier-Stokes solver. Ogura and Utsunomiya⁵⁾ solved the viscous flows around a floating body subject to heave and roll motions by using the Navier-Stokes solver. But for the applications to large motion amplitudes, convergence is still difficult to gain. Further investigation of the hydrodynamic coefficients of a floating body undergoing roll motions is considered to be necessary. Thus, a new numerical method to solve the Navier-Stokes equations is still necessary to be developed. In this research, a finite volume method incorporated with moving unstructured grids is the selected numerical approximation.

2. Two-dimensional Navier-Stokes Solver

2.1 Governing Equations

The governing equations employed in the computational domain are the conservation law of mass and the conservation law of momentum,

$$\frac{\partial u_i}{\partial x_i} = 0, \quad (1)$$

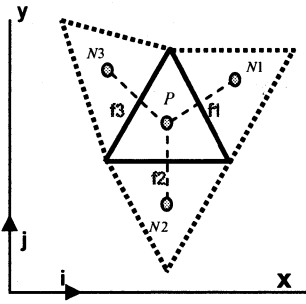


Fig.1 Geometry details of cell center based scheme

$$\rho \frac{\partial u_i}{\partial t} + \rho u_j \frac{\partial u_i}{\partial x_j} = \mu \frac{\partial^2 u_i}{\partial x_j \partial x_j} + \rho X_i - \frac{\partial p}{\partial x_i}, \quad (2)$$

where u_i represents the total velocity vector, x_i the spatial coordinates, t the time, ρ the density of the fluid, μ the viscosity of the fluid, X_i the body force per unit volume, and p the pressure. In the following formulations, ρ is considered to be a constant, and the body force X_i is neglected.

2.2 Finite Volume Method

In the cell center based finite volume method, the Navier-Stokes equations in Eq. (2) can be written in the following semi-discrete integral form.

$$\begin{aligned} & \left(\rho \frac{\partial u_i}{\partial t} \right)_P \Delta \Omega_P + \sum_{m=1}^{N_{face}} (\rho u_i n_j)_{f_m} S_{f_m} \\ & = \sum_{m=1}^{N_{face}} \left(\mu \frac{\partial u_i}{\partial x_j} n_j \right)_{f_m} S_{f_m} - \left(\frac{\partial p}{\partial x_i} \right)_P \Delta \Omega_P. \end{aligned} \quad (3)$$

Here, $\Delta \Omega_P$ is the volume of the cell (or the control volume) P , S_{f_m} the area of the cell surface f_m and $(n_j)_{f_m}$ the outward normal vector at the cell surface. The geometry details of the cell P and its neighbors N_1 , N_2 , N_3 are shown in Fig. 1. The convective flux in Eq. (3) is approximated by the midpoint rule integration. The midpoint rule itself has the second-order accuracy⁶⁾.

$$(F_i^C)_{f_m}^k = \left(\int_{S_{f_m}} \rho u_i n_j dS \right)^k \approx (\dot{m}^{k-1} u_i^k)_{f_m}, \quad (4)$$

$$\dot{m}_{f_m}^k = \left(\int_{S_{f_m}} \rho u_j n_j dS \right)^k \approx (\rho u_j S_j)_{f_m}^k, \quad (5)$$

where $\dot{m}_{f_m}^k$ is the mass flux passing through the cell surface f_m at the iterative step k . The symbol $(S_j)_{f_m}$ is defined by $(S_j)_{f_m} = S_{f_m} (n_j)_{f_m}$.

To avoid convergence problem during the iteration, the deferred correction approach is used to interpolate the convective flux at the cell face center f_m :

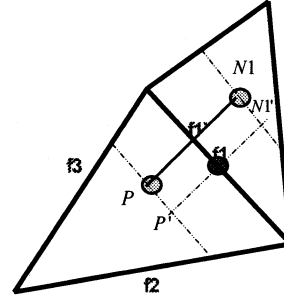


Fig.2 Irregularity in unstructured grids

$$\begin{aligned} (F_i^C)_{f_m}^k & = (\dot{m}^{k-1} u_i^k)_{f_m}^{UDS} \\ & + \beta \left[(\dot{m}^{k-1} u_i^{k-1})_{f_m}^{CDS} - (\dot{m}^{k-1} u_i^{k-1})_{f_m}^{UDS} \right], \end{aligned} \quad (6)$$

$$(\dot{m}^{k-1} u_i^k)_{f_m}^{UDS} = \max(\dot{m}_{f_m}^{k-1}, 0) u_{i,P}^k + \min(\dot{m}_{f_m}^{k-1}, 0) u_{i,N_m}^k, \quad (7)$$

$$(\dot{m}^{k-1} u_i^{k-1})_{f_m}^{UDS} = \max(\dot{m}_{f_m}^{k-1}, 0) u_{i,P}^{k-1} + \min(\dot{m}_{f_m}^{k-1}, 0) u_{i,N_m}^{k-1}, \quad (8)$$

where UDS and CDS mean the upwind difference scheme and the central difference scheme, respectively. β is a blending factor which determines the interpolation scheme. The range of the blending factor is $0 \leq \beta \leq 1$. $\beta = 1$ is for central difference scheme and $\beta = 0$ is for upwind scheme. In the numerical examples presented below, $\beta = 0$ is used.

Interpolating the velocity field at the cell face f_1 by linear interpolation assumes that the line connecting nodes P and N_1 passes through the cell face center f_1 . In that case the approximation of the surface integral is second-order accurate. When the grid is irregular, the line connecting nodes P and N_1 may not pass the cell face center. In order to preserve the second-order accuracy of the midpoint rule, we use the values at auxiliary nodes P' and N_1' instead of those at nodes P and N_1 , see Fig. 2. Thus, the convective flux approximated by the central difference scheme is modified to include the irregularity term in order to keep the second-order accuracy.

$$\begin{aligned} (u_i^k)_{f_m}^{CDS} & = (1 - \lambda_{f_m}) (u_i^k)_P + \lambda_{f_m} (u_i^k)_{N_m} \\ & + \left(\frac{\partial u_i}{\partial x_j} \right)_{f_m}^k \{ (x_j)_{f_m} - (x_j)_{f_m'} \}, \end{aligned} \quad (9)$$

$$\lambda_{f_m} = \frac{L_{f_m',P}}{L_{N_m,P}}, \quad (10)$$

where $L_{N_m,P}$ is the distance between cell centers N_m and P , and $L_{f_m',P}$ the distance between f_m' and P .

Approximation of diffusive fluxes requires the values of gradient of u_i in the direction normal to cell face.

$$\begin{aligned} (F_i^D)_{fm}^k &= \left(\int_{S_{fm}} \mu \frac{\partial u_i}{\partial x_j} n_j dS \right)^k \approx \left(\mu \frac{\partial u_i}{\partial x_j} n_j \right)_{fm}^k S_{fm} \\ &= \frac{\mu S_{fm}}{L_{Nm,P}} \left\{ (u_i^k)_{Nm} - (u_i^k)_P \right\}. \end{aligned} \quad (11)$$

By using the Gauss' theorem, one can approximate the gradients at the cell center and interpolate them to the cell faces. The gradients at the cell center are approximated by the average value over the cell:

$$\begin{aligned} \left(\frac{\partial u_i}{\partial x_j} n_j \right)_P &\approx \frac{\int_{\Omega} \frac{\partial u_i}{\partial x_j} n_j d\Omega}{\Delta\Omega_P} = \frac{\sum_{m=1}^{N_{face}} \int_{S_{fm}} u_i n_j n_j dS}{\Delta\Omega_P} \\ &= \frac{\sum_{m=1}^{N_{face}} \int_{S_{fm}} u_i dS}{\Delta\Omega_P} = \frac{\sum_{m=1}^{N_{face}} (u_i S)_{fm}}{\Delta\Omega_P}. \end{aligned} \quad (12)$$

Due to oscillation problem during the iteration procedure, diffusive flux is approximated by applying the deferred-correction term as follows:

$$(F_i^D)_{fm}^k = (F_i^{D,impl})_{fm}^k + \left[(F_i^{D,expl})_{fm}^{k-1} - (F_i^{D,impl})_{fm}^{k-1} \right], \quad (13)$$

The term of 'impl' here denotes the implicit, and 'expl' denotes the explicit flux approximation. Approximation of the implicit term is calculated by Eq. (11), and approximation of the explicit term is:

$$\begin{aligned} (F_i^{D,expl})_{fm}^k &= \mu \left(S \frac{\partial u_i}{\partial x_j} n_j \right)_{fm} \\ &= \mu S_{fm} \left[(1 - \lambda_{fm}) \left(\frac{\partial u_i}{\partial x_j} n_j \right)_P + \lambda_{fm} \left(\frac{\partial u_i}{\partial x_j} n_j \right)_{Nm} \right]. \end{aligned} \quad (14)$$

The pressure term in the momentum equation is approximated by the midpoint rule integration:

$$Q_i^p = - \int_{\Omega} \frac{\partial p}{\partial x_i} d\Omega \approx - \left(\frac{\partial p}{\partial x_i} \right)_P \Delta\Omega_P. \quad (15)$$

The unsteady term is discretized by using the implicit three-time level method:

$$\left[\frac{\partial}{\partial t} \int_{\Omega} \rho u_i d\Omega \right]_P \approx \frac{\rho \Delta\Omega_P}{2\Delta t} (3u_i^{n+1} - 4u_i^n + u_i^{n-1})_P. \quad (16)$$

Here, the upper-script n indicates the time step, and $\Delta t = t^{n+1} - t^n$ is the time interval.

The body moves every time step, therefore the grids attached at the body have to move as far as the body movements. If the flux change due to moving grids is accounted in the computation, the velocity in the convective flux term is not the total velocity but the relative velocity and the modified

momentum equation is,

$$\rho \frac{\partial u_i}{\partial t} + \rho (u_j - u_j^{grid}) \frac{\partial u_i}{\partial x_j} = \mu \frac{\partial^2 u_i}{\partial x_j \partial x_j} + \rho X_i - \frac{\partial p}{\partial x_i}, \quad (17)$$

where grid velocity is expressed in the following equations,

$$u_j^{grid} = \frac{x_j^n - x_j^{n-1}}{\Delta t}. \quad (18)$$

2.3 Pressure-Correction Scheme

The pressure-correction scheme based on SIMPLE⁷⁾ algorithm is applied to couple the momentum equations with the continuity equation. The predicted values, u_i^{k*} obtained from the linearized momentum equation have to be corrected so that mass at each control volume is conserved.

$$u_i^k = u_i^{k*} + u_i', \quad (19)$$

$$p^k = p^{k-1} + p', \quad (20)$$

where u_i' and p' are the correction terms for the velocity and the pressure. These values are determined such that the following mass conservation at each control volume is satisfied:

$$\sum_{m=1}^{N_{face}} \dot{m}_{fm} = \sum_{m=1}^{N_{face}} \dot{m}_{fm}^{k*} + \sum_{m=1}^{N_{face}} \dot{m}'_{fm} = 0. \quad (21)$$

In the actual implementation to the computer program, an approach invented by Rhie and Chow⁸⁾ is used.

2.4 Boundary Conditions

The boundary conditions for a floating body oscillating at a frequency ω in otherwise calm water (without incident wave) are given in Ogura and Utsunomiya⁵⁾. In the following, the x -axis is taken horizontally on the free surface, and the y -axis taken vertically upward. The velocity components in the x - and y -axes are given by the symbols u and v , respectively.

(1) Free surface boundary

From the linearized kinematic and dynamic free surface boundary conditions, one can obtain

$$\frac{\partial u}{\partial x} = \frac{\omega^2}{g} u, \quad \frac{\partial v}{\partial y} = \frac{\omega^2}{g} v. \quad (22)$$

Using the linearized Bernoulli's equation, one obtains

$$\frac{\partial p}{\partial t} = \rho g v, \quad (23)$$

where g is the gravity acceleration. Note that these conditions are applied on the undisturbed free surface, i.e., on $y = 0$.

(2) Far boundary

At the far boundary, there is no fluid particle movement. Thus,

$$u = v = 0, \quad (24)$$

$$\frac{\partial p}{\partial n} = 0. \quad (25)$$

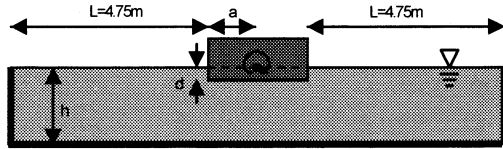


Fig. 3 Numerical model

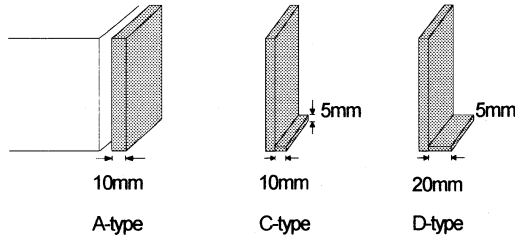


Fig. 4 Configurations of the bilge keels

Table 1 Dimensions of the model

Water Depth, h	0.5m
Half-Beam Length, a	0.25m
Draft, d	0.05m
Center of Gravity, Z_{G1}	0.025m
Roll Center, Z_{C1}	0.0m
Viscosity, μ	0.001 N/ms

(3) Hull surface

At the hull surface, the velocity of the floating body is assigned:

$$u = u_{hull}(t), \quad v = v_{hull}(t), \quad (26)$$

where $u_{hull}(t)$ and $v_{hull}(t)$ are the velocity components of the hull surfaces. The pressure working at the hull surface may be given as,

$$\frac{\partial p}{\partial n} = -\rho \left(\frac{\partial u_n}{\partial t} + u_n \frac{\partial u_n}{\partial n} + u_s \frac{\partial u_s}{\partial s} \right), \quad (27)$$

where n is the normal direction and s the tangential direction on the hull surface.

3. Numerical Results and Discussions

3.1 Numerical Model

A 2D floating barge with its boundary conditions is modeled to approximate the real condition in calm water. The numerical model used in our computation is depicted in Figs. 3 and 4. The dimensions of the hull section and the boundary length are shown in Table 1. A floating hull with or without bilge keels is presented here. The A-type barge has sharp edges without bilge keels. The C-type barge has horizontal bilge keels of 10mm length and 5mm thickness. The D-type barge has horizontal bilge keels of 20mm length and 5mm thickness. In Figs. 5 and 6, the details of the grid construction used for the analysis of A-type barge and C-type barge are shown. The number of elements for A-type barge is 6534 (384 for structured mesh and 6158 for unstructured mesh) and that for C-type barge is 7554 (unstructured mesh only).

The harmonic roll motions around the center of floatation are given:

$$\alpha = A_0 \sin \omega t. \quad (28)$$

The range of oscillation frequencies, f , is from 0.8 Hz to 1.7 Hz, and the range of roll angles, A_0 , from 0.01 rad to 0.04 rad. The initial conditions are specified as $u = v = 0$ and $p = 0$ for entire fluid domain.

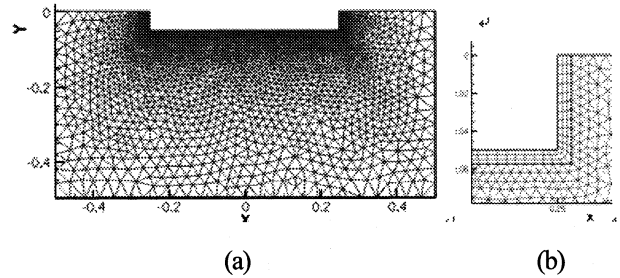


Fig. 5 (a) Grid construction around A-Type barge, (b) Close-up view of grid around the corner of hull section.

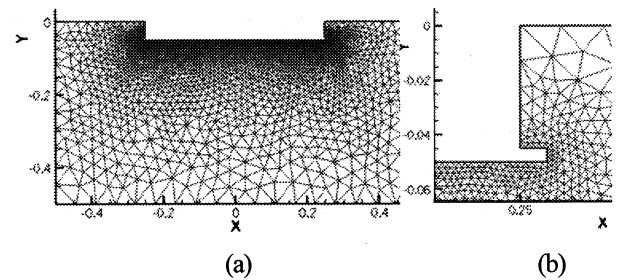


Fig. 6 (a) Grid construction around C-Type barge, (b) Close-up view of grid around the corner of hull section.

3.2 Roll Hydrodynamic Coefficients

The moment working on the center of floatation due to roll motion is calculated by

$$M = - \int_S p(xn_y - yn_x) dS, \quad (29)$$

where S is the wetted-surface of the floating body, and (n_x, n_y) is the outward normal vector on the body surface. In the viscous fluid, the viscous stress components also affect the resulting moment. However, Yeung and Ananthkrishnan⁹ showed that the pressure component is much larger than the viscous components; the shear-stress contribution is about 10%, and the normal-stress contribution is only about 1% of the pressure components for a heaving body. Thus, the viscous stress components are neglected in the calculation of the moment acting on the floating body, as has usually been made in similar studies^{2)-5),9)}.

Fig. 7 shows the moment histories at $f = 1.7$ Hz for A-type and C-type barges. As can be seen in Fig. 7, the moment histories can be fitted well with the following harmonic curve:

$$M = M_0 \sin(\omega t + \beta), \quad (30)$$

where M_0 is the moment amplitude and β the phase angle with respect to the roll excitation. According to the linear theory, the hydrodynamic roll moment can be written as a linear combination of the inertia and damping terms.

$$M = -a_{44}\ddot{\alpha} - b_{44}\dot{\alpha}, \quad (31)$$

where a_{44} is the roll added mass and b_{44} the roll damping coefficient. Substituting Eq. (28) into Eq. (31), and equating it with Eq. (30), one obtain,

$$a_{44} = M_0 \cos \beta / (A_0 \omega^2), \quad (32)$$

$$b_{44} = -M_0 \sin \beta / (A_0 \omega). \quad (33)$$

In Figs. 8-10, the roll added mass and the roll damping coefficient evaluated by the N-S solver are plotted for non-dimensionalized wave number, ka (k : wave number, a : half width of the floating body). In the same figures, the roll added

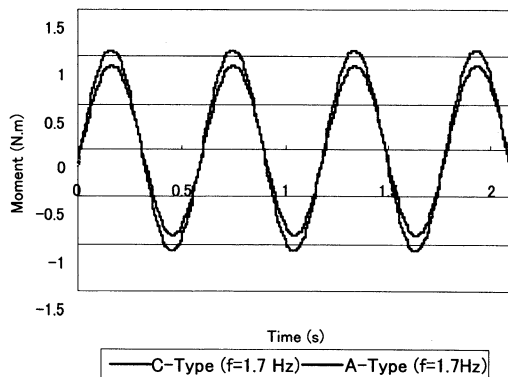
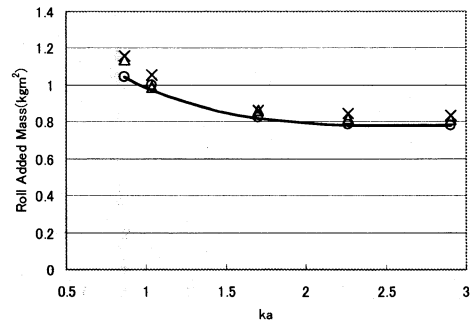
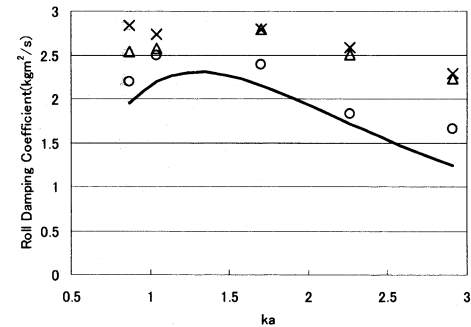


Fig. 7 Comparison of the moment histories between C-type and A-type barge

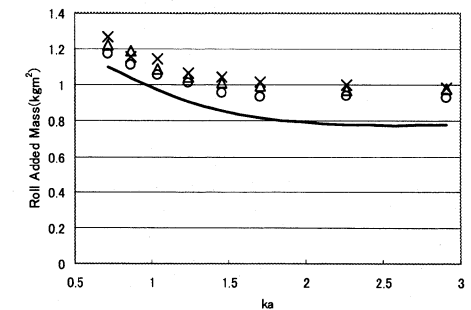


(a) Roll added mass

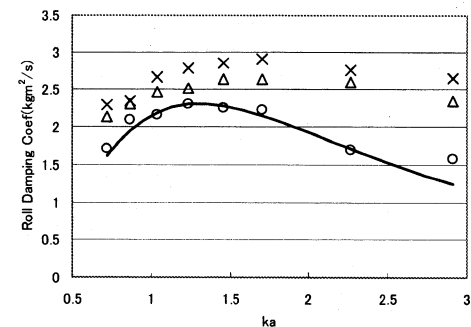


(b) Roll damping coefficient

Fig. 8 Roll added mass (a) and damping coefficient (b) of A-type barge ($A_0 = 0.01$ rad – 0.04 rad)

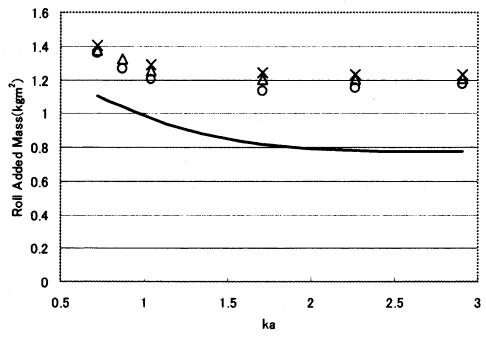


(a) Roll added mass

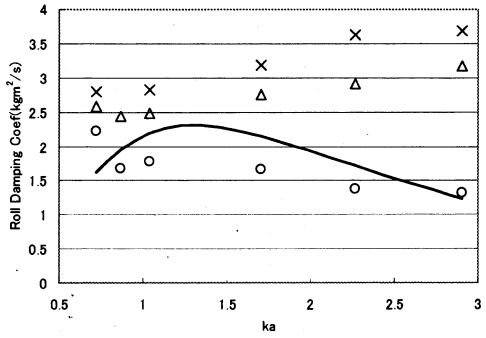


(b) Roll damping coefficient

Fig. 9 Roll added mass (a) and damping coefficient (b) of C-type barge ($A_0 = 0.01$ rad – 0.04 rad)



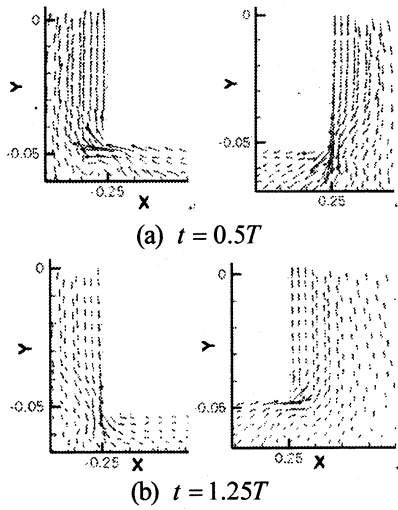
(a) Roll added mass



(b) Roll damping coefficient

○ D-Type ($A_0 = 0.01$ rad), N-S Solver △ D-Type ($A_0 = 0.03$ rad), N-S Solver
 × D-Type ($A_0 = 0.04$ rad), N-S Solver — A-Type, Linear Potential Theory

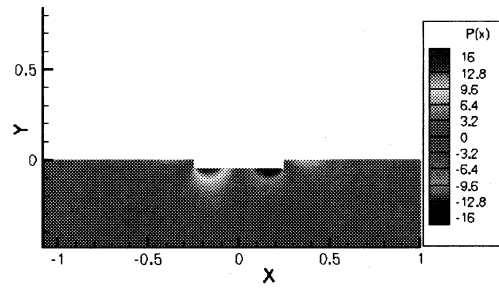
Fig. 10 Roll added mass (a) and damping coefficient (b) of D-type barge ($A_0 = 0.01$ rad – 0.04 rad)



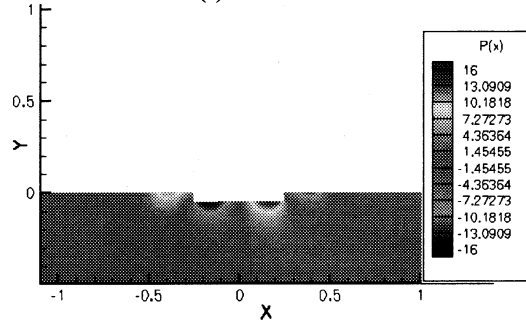
(a) $t = 0.5T$

(b) $t = 1.25T$

Fig. 11 The velocity vectors around A-type barge predicted by N-S solver at different times ($A_0 = 0.01$ rad)

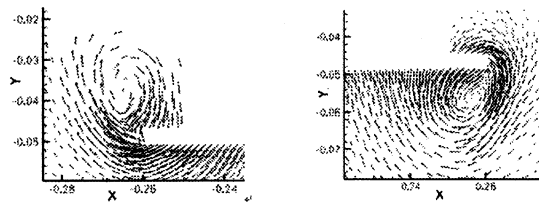


(a) $t = 0.5T$

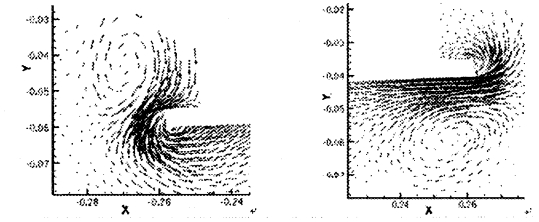


(b) $t = 1.25T$

Fig. 12 The pressure contour plots of A-type barge predicted by N-S solver at different times ($A_0 = 0.01$ rad)



(a) $t = 1.0T$



(b) $t = 2.25T$

Fig. 13 The velocity vectors around C-type barge predicted by N-S solver at different times ($A_0 = 0.04$ rad)

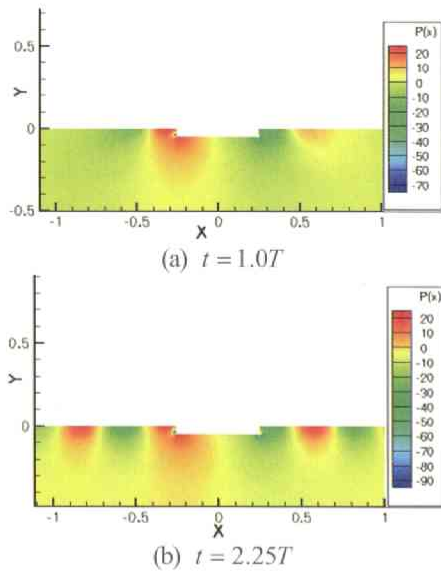


Fig. 14 The pressure contour plots of C-type barge predicted by N-S solver at different times ($A_0 = 0.04$ rad)

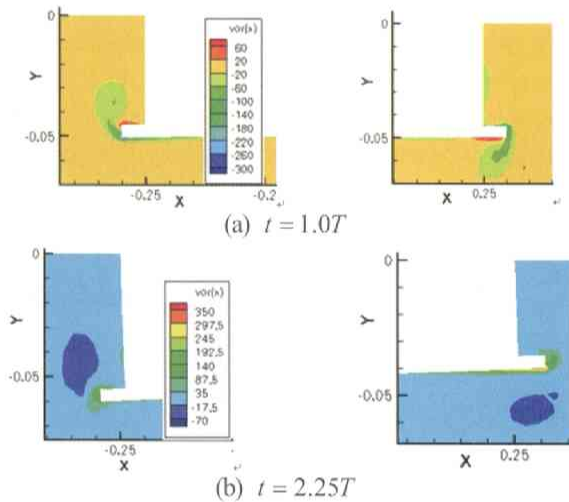


Fig. 15 The vorticity contour plots of C-type barge predicted by N-S solver at different times ($A_0 = 0.04$ rad)

mass and the roll radiation damping coefficient evaluated by the linear potential theory are plotted for comparison. The reasons why the hydrodynamic coefficients computed by the presented scheme are compared with those derived by the potential theory are 1) the potential theory is most frequently employed and most established for evaluation of hydrodynamic forces acting on a hydrodynamically compact structure¹⁰⁾, and 2) the effect of viscosity and vorticity in the roll damping coefficient may be captured as the difference between both methods.

When bilge keels installed, the flow separates at the tip of the bilge keels, and it modifies significantly the moment (Fig. 7). Downie et al.¹¹⁾ studied on the effect of vortex shedding on the hydrodynamic damping of a floating barge undergoing forced roll motion. The results show that for a floating body with sharp edges and appendages, the damping coefficients due to vortex

shedding is proportional to the square of both the frequency and amplitude of the motion. This is consistent with the numerical results obtained in this research in terms of the non-linear manner of the damping coefficients with respect to the roll angle and also frequency of motion (Figs. 8-10).

The resulting damping coefficients evaluated in this research also show the same trend with the roll-damping coefficients presented by Kinnas et al.⁴⁾. As the roll angle of a floating body increases, the damping coefficient increases significantly (Figs. 8(b)-10(b)). The values of added mass also change as the roll angle increases but they do not change substantially as much as in the case of roll damping (Figs. 8(a)-10(a)). This significance is more severe if the hull installed with bilge keels.

3.3 Prediction of Flow Field around Floating Sections

The predicted velocity vectors and vorticity contour plots around the A-type barge and C-type barge oscillating with frequency of 1.7 Hz are plotted in Figs. 11-15. The pressure contour plots are also presented to show the linear free surface condition at the mean surface of water.

It can be seen from Fig.11 that large velocity vectors around the A-type barge exist near the corner of the hull section. Small vortices are also generated but stronger vortices are generated near the corner of the floating hull fitted with bilge keels. The vortex becomes stronger when the roll angle increases (Fig.15).

The plots show that the developed vortex is located behind the moving direction of the structure (Fig.13). If the structure rolls away (counterclockwise), a strong negative (clockwise) vortex exists to damp out the rolling motion. The vortex rolls in a counterclockwise way when the structure rolls in (clockwise). The developed vortex alters the pressure distribution, and thus results in larger damping coefficients than predicted by the linear potential theory.

4. Conclusions

In the current work, the Navier-Stokes solver has been developed, and applied for laminar flows. The free surface condition is approached by using the linear wave theory. The structure is under roll motions with different roll angles and the dependence of the resulting hydrodynamic coefficients are investigated. The numerical results show that the values of the added mass and damping coefficients depend on the amplitude of the roll motion. The viscosity also affects the non-linear behavior of the moment amplitudes as well as the phase differences with respect to the angle of roll. This non-linear behavior is more significant at larger roll amplitudes.

The results of added mass predicted by using the Navier-Stokes solver compare well with those obtained from the linear potential theory in both cases, a floating body with or without bilge keels. This shows that the values of added mass are not influenced by fluid viscosity. But significant results are

obtained for values of damping coefficients. Fluid viscosity affects the flow especially near the boundary layers and therefore, increases the values of damping coefficients. This indicates that viscosity plays important role for problems of floating bodies subject to roll motions. The validation of the added mass and damping coefficients by comparison with the experiment is under way, and will be presented in a near future.

Acknowledgement

This study has been carried out as a part of "Research and Development of Offshore Platform" of an entrusted research from Ministry of Land, Infrastructure, Transport and Tourism. The authors give our great thanks to persons concerned.

References

- 1) Chakrabarti, S., Empirical calculation of roll damping for ships and barges, *Ocean Engineering* 28, pp.915-932, 2001.
- 2) Yeung, R. W., Liao, S.-W. and Roddier, D., Hydrodynamic coefficients of rolling rectangular cylinders, *Int. Journal of Offshore and Polar Engineers*, 8, pp. 241-250, 1998.
- 3) Yeung, R. W., Fluid dynamics of finned bodies – From VIV to FPSO, *Proc. 12th Int. Offshore and Polar Engineering Conf.*, Kitakyushu, Japan, pp. 1-11, 2002.
- 4) Kinnas, S. A., Yu, Y.-H., and Vinayan, V., Prediction of flows around FPSO hull sections in roll using an unsteady Navier-Stokes solver, *Proc. 16th Int. Offshore and Polar Engineering Conf.*, San Fransisco, USA, pp. 384-392, 2006.
- 5) Ogura, H., and Utsunomiya, T., A Navier-Stokes solver for dynamic response prediction of an oscillating floating body, *Journal of Applied Mechanics*, JSCE, 10, pp. 1081-1088, 2007.
- 6) Ferziger, J.H. and Peric, M., *Computational Methods for Fluid Dynamics*, Springer-Verlag, Berlin, 1996.
- 7) Patanker, S., *Numerical Heat Transfer and Fluid Flow*, McGraw-Hill, New York, 1980.
- 8) Rhie, C. M. and Chow, W. L., Numerical study of the turbulent flow past an airfoil with trailing edge separation, *AIAA Journal*, 21, pp.1525-1532, 1983.
- 9) Yeung, R. W. and Ananthakrishnan, P., Oscillation of a floating body in a viscous fluid, *Journal of Engineering Mathematics*, 26, pp. 211-230, 1992.
- 10) Clauss, G., Lehmann, E., and Oestergaard, C., *Offshore Structures, Vol. 1, Conceptual Design and Hydromechanics*, Springer-Verlag, 1991.
- 11) Downie, M. J., Bearman, P. W., and Graham J. M. R., Effect of vortex shedding on the coupled roll response of bodies in waves, *Journal of Fluid Mechanics*, pp. 243-264, 1987.

(Received: April 14, 2008)